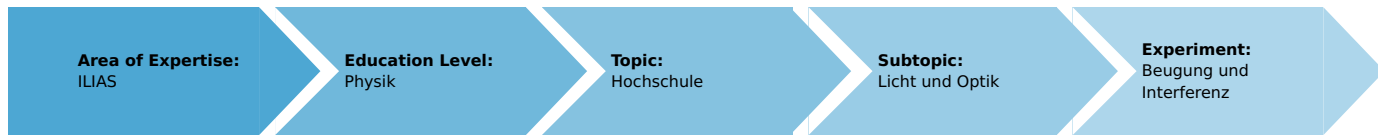


Fabry-Perot interferometer - optical resonator modes

(Item No.: P2221206)

Curricular Relevance



Difficulty



Difficult

Preparation Time



10 Minutes

Execution Time



20 Minutes

Recommended Group Size



2 Students

Additional Requirements:

Experiment Variations:

Keywords:

Interference, wavelength, diffraction index, speed of light, phase, virtual light source, two-beam interferometer

Introduction

overview

Principle

Two mirrors are assembled to form a Fabry-Perot Interferometer. Using them, the multibeam interference of a laser's light beam is investigated. On moving one of the mirrors, the change in the intensity distribution of the interference pattern is studied. This is a qualitative experiment, to study the shape of different laser modes and compare it with some photos given in this description.

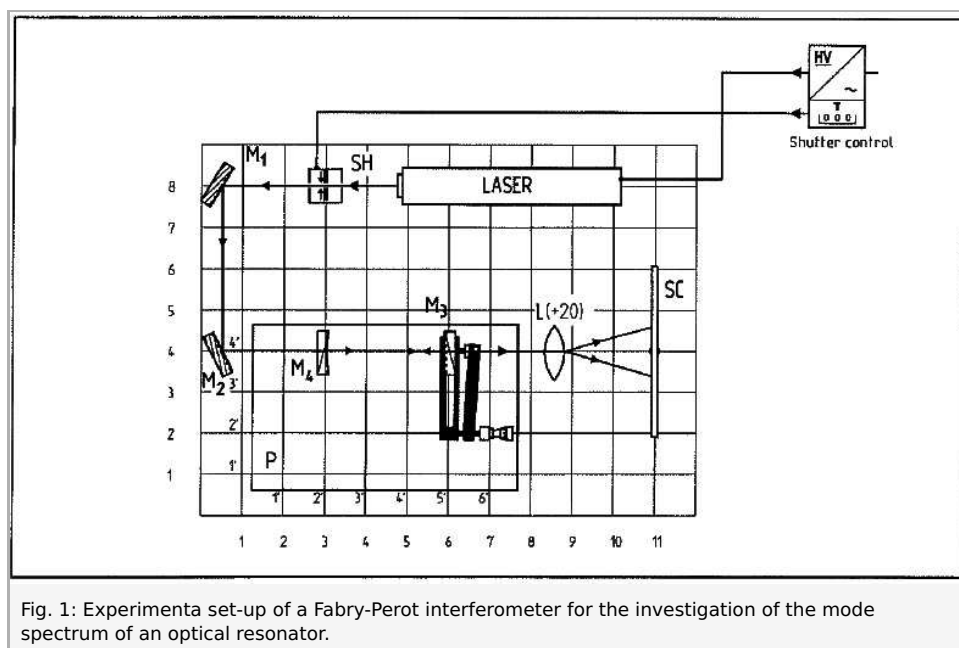


Fig. 1: Experimenta set-up of a Fabry-Perot interferometer for the investigation of the mode spectrum of an optical resonator.

Equipment

Position No.	Material	Order No.	Quantity
1	Optical base plate with rubber feet	08700-00	1
2	Interferometer plate with precision drive	08715-00	1
3	Adjusting support 35 x 35 mm	08711-00	4
4	Surface mirror 30 x 30 mm	08711-01	2
5	Concave mirror OC; $r = 1.4 \text{ m}$, $T = 1.7\%$	08711-03	1
6	Plane mirror HR > 99%, mounted	08711-02	1
7	Magnetic foot for optical base plate	08710-00	5
8	Lens, mounted, $f +20 \text{ mm}$	08018-01	1
9	Lensholder for optical base plate	08723-00	1
10	Screen, white, 150x150 mm	09826-00	1
11	He/Ne Laser, 5 mW with holder	08701-00	1
12	Power supply for laser head 5 mW	08702-93	1

Tasks

1. Construction of a Fabry-Perot interferometer using separate optical components.
2. The interferometer is used to observe different resonator modes within the interferometer.

Set-up and procedure

In the following, the pairs of numbers in brackets [...] refer to the co-ordinates on the optical base plate. These coordinates are only intended to be a rough guideline for making initial adjustments.

- Perform the experimental set-up according to Fig. 1. The recommended set-up height (beam path height) is **130 mm**.
- Initially, perform the adjustment work without the lens $L[8.5, 4]$. Before beginning with the adjustments, place the fine-adjusting drive on auxiliary plate **P** onto the optical base plate in accordance with Fig. 1. While doing so ensure that the coordinate lines on the auxiliary plate align as exactly as possible with those on the base plate.
- When adjusting the beam path with the adjustable mirrors $M_1[0.5, 8]$ and $M_2[0.5, 4]$ at beam path height, align the beam along the 4th y coordinate of the optical base plate.
- To begin with, position mirror $M_3[6, 4] = [5', 4']$ (plane mirror with a 99% reflection factor). Place the mirror in the holder of the adjusting support. Then adjust mirror M_3 such that the reflected beam strikes the same point on mirror M_2 from which is originated.
- Take the concave mirror (concave mirror with a radius of curvature of **1400 mm**) and attach it to the adjusting support. Place this mirror, $M_4[3, 4] = [2', 4']$ with its metallized side facing M_3 in the beam path in such a manner that the beam reflected by M_4 is incident to mirror M_3 .
- Mirror M_4 must be fine-adjusted such that the reflected beam approximately coincides with its point of origin on mirror M_3 .
- By altering the distance separating the two interferometer mirrors M_3 and M_4 by means of turning the micrometer screw (on the mirror support of plate **P**), one obtains a luminous point on screen $SC[11, 4]$.
- The light beam is expanded by placing the lens $L[8.5, 4]$ in the beam path.
- Now, one probably can see patterns (see Figs. 7 and 8) on the screen as a result of the different amplitude distributions of resonator modes in the interferometer.
- By painstakingly readjusting the parallelism of the mirrors, one obtains symmetrical patterns. When a small ellipse occurs, try to minimize the size to a point! If this is not possible, realign the whole set-up. The alignment is okay, when a flickering spot can be seen. Please also loose the screw, which holds the mirror M_4 in its mounting and turn the mounting around the optical axis for further alignment.
- On making the smallest possible changes in the interferometer's length (using the micrometer screw), one sees an alteration of the modes, whereby the radial extension increases with increasing order. If the laser has only been switched on shortly before the experiment, alteration of the modes can already be seen without changing the interferometers length, as the frequency of the laser resonator changes due to thermal expansion. This effect also takes place, when the laser set-up is effected by vibrations of the table or the ground. Alterations of modes can also be caused by thermal instabilities of the Fabry-Perot-Resonator or due to dust in the laser beam.

Theory and evaluation

The Michelson interferometer (as well as the MachZehnder and Sagnac interferometer) is a twobeam interferometer. In general, in these cases, two light waves having different frequencies are superimposed with differing amplitudes. In contrast, the Fabry-Perot interferometer is a multibeam interferometer. An ideal Fabry-Perot interferometer consists of two plane-parallel light-absorbing glass plates (mirrors) which are separated by distance d . Since the absorption can be neglected, the following is true for the reflection R :

$$R = 1 - T \text{ (where } T = \text{transmittance).}$$

The principle of the Fabry-Perot interferometer:

The principle of the interferometer is illustrated in Fig.2. The input wave has amplitude a_0 and thus the intensity $a_0^2 = I_0$. Behind the first glass plate, the intensity is:

$$I_1 = (1 - R) \cdot I_0 = T \cdot I_0 \tag{1}$$

Accordingly, the amplitude is:

$$a_{i1} = \sqrt{1 - R} \cdot a_0 \tag{2}$$

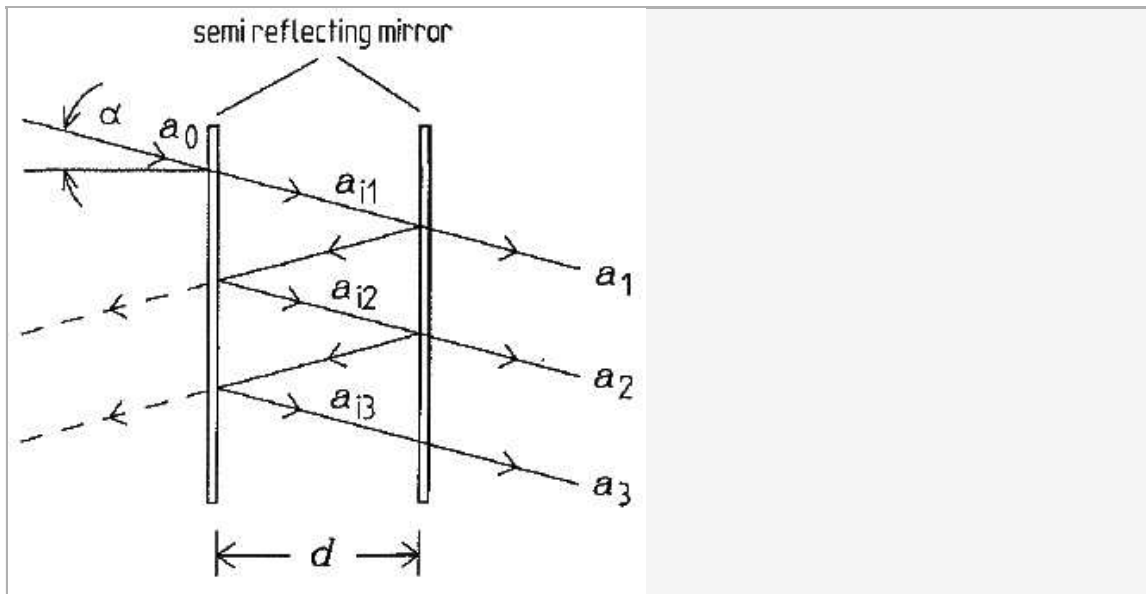


Fig. 2: Multibeam interferometer after Fabry and Perot. Illustration of the principle for deriving the individual amplitudes.

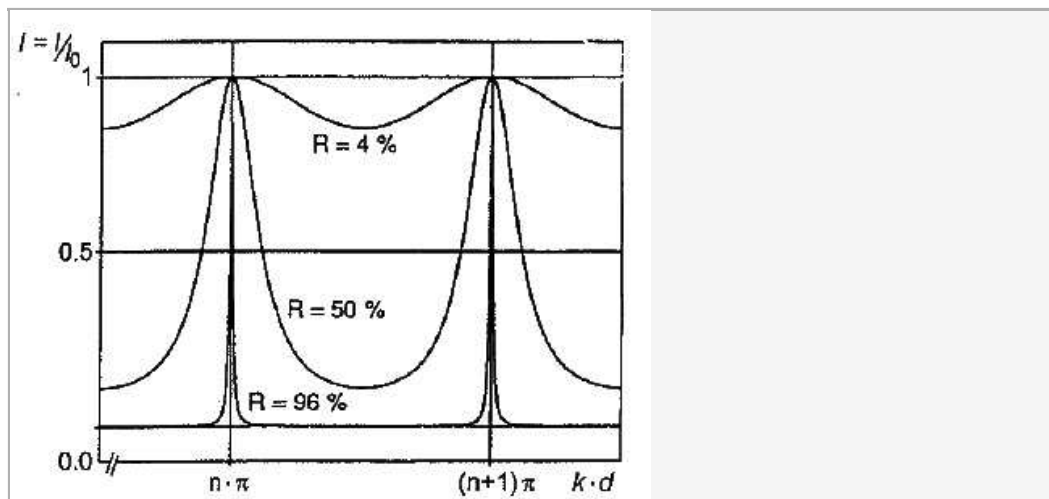


Fig. 3: The transmission curve T_1 of a Fabry-Perot interferometer for various reflection factors R of the mirror.

For the subsequent reflections of the wave between the glass plates, the following results:

$$\begin{aligned}
 a_{i2} &= R \cdot a_{i1} = \sqrt{1-R} \cdot R^1 \cdot a_0 \\
 a_{i3} &= R \cdot a_{i2} = \sqrt{1-R} \cdot R^2 \cdot a_0 \\
 a_{i4} &= R \cdot a_{i3} = \sqrt{1-R} \cdot R^3 \cdot a_0 \\
 &\vdots \\
 a_{in} &= R \cdot a_{i(n-1)} = \sqrt{1-R} \cdot R^{n-1} \cdot a_0
 \end{aligned}$$

In this case the partial beams emerging from the second plate have the following amplitudes:

$$\begin{aligned}
 a_1 &= \sqrt{1-R} \cdot a_{i1} = (1-R) \cdot a_0 \\
 a_2 &= \sqrt{1-R} \cdot a_{i2} = (1-R) \cdot R^1 \cdot a_0 \\
 a_3 &= \sqrt{1-R} \cdot a_{i3} = (1-R) \cdot R^2 \cdot a_0 \\
 &\vdots \\
 a_n &= \sqrt{1-R} \cdot a_{in} = (1-R) \cdot R^{n-1} \cdot a_0
 \end{aligned}$$

If we now consider a time- and place-independent oscillation where:

$$E = a \cdot \cos(\omega t + kx + \delta)$$

and where E_1 is the first partial wave that has passed through the two glass plates, then the phase δ of the phase difference of the subsequent partial beams, which are generated by the different path lengths of the light through the Fabry-Perot interferometer, is as follows:

$$\delta = \frac{2 \cdot k \cdot d}{\cos \alpha}$$

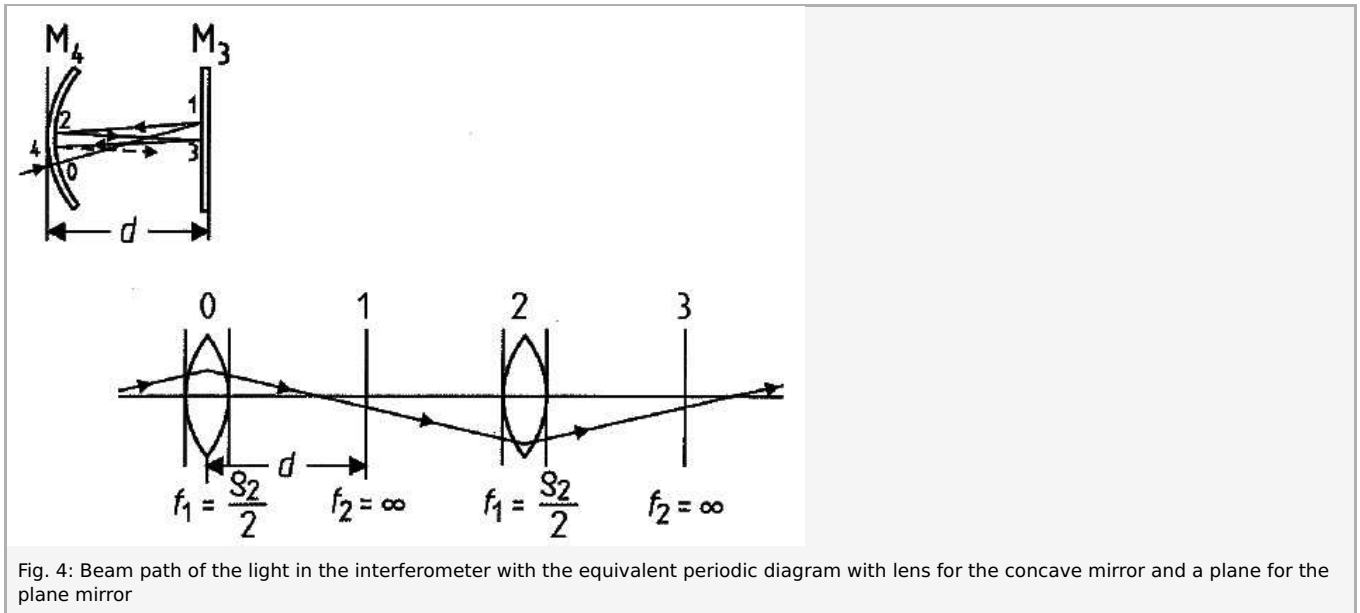


Fig. 4: Beam path of the light in the interferometer with the equivalent periodic diagram with lens for the concave mirror and a plane for the plane mirror

Consequently, the following equation results for the individual emerging partial beams:

$$\begin{aligned}
 E_1 &= a_1 \cdot \cos(\omega t + k \cdot x) & (3) \\
 E_2 &= a_2 \cdot \cos(\omega t + k \cdot x + \delta) \\
 E_3 &= a_3 \cdot \cos(\omega t + k \cdot x + 2 \cdot \delta) \\
 &\vdots \\
 E_n &= a_n \cdot \cos(\omega t + k \cdot x + (n-1) \cdot \delta)
 \end{aligned}$$

$$E_n = (1 - R) \cdot R^{n-1} \cdot a_0 \cdot \cos(\omega t + k \cdot x + (n - 1) \cdot \delta)$$

The resulting amplitude E is the sum of the individual amplitudes E_n :

$$E = \sum_{n=1}^{\infty} E_n$$

with $\cos \alpha = \text{Re}[e^{i\alpha}]$, the intensity of the resulting light wave is obtained from

$$I = E \cdot E^* \quad (4)$$

(where E^{ast} is the conjugated complex)

For p reflections between the plates, the following results for the amplitude according to Equation (3):

$$E = \text{Re}\{e^{i(\omega t + kx)} \cdot (1 - R)a_0 \sum_{n=2}^p R^{n-1} \cdot e^{i(n-1)\delta}\} \quad (5)$$

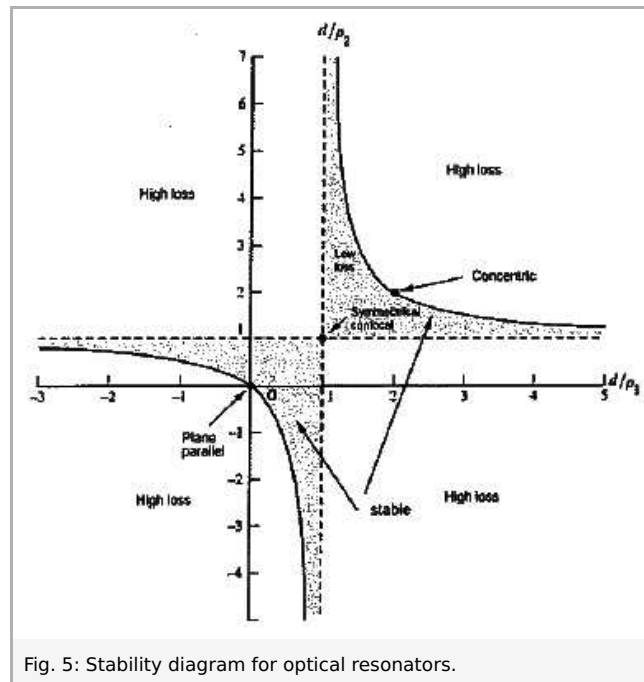


Fig. 5: Stability diagram for optical resonators.

The sum is a geometric series:

$$\sum_{m=1}^p R^m \cdot e^{im\delta} = \frac{1 - p \cdot R \cdot e^{ip\delta}}{1 - R \cdot e^{i\delta}}$$

following results for the total field strength E :

$$E = \text{Re}\{e^{i(\omega t + kx)} \cdot (1 - R)a_0 \frac{1}{1 - R \cdot e^{i\delta}}\} \quad (6)$$

In the formation of the limit, $p \rightarrow \infty$, $p \cdot R$ approaches zero, since $R < 1$.

The intensity results from Equation (4) as:

$$I = I_0 \cdot \frac{(1 - R)^2}{(1 - R \cdot e^{i\delta}) \cdot (1 - R \cdot e^{-i\delta})}$$

After further rearrangement, the following is the obtained:

$$I = I_0 \cdot \frac{(1 - R)^2}{(1 - R)^2 + 4 \cdot R \cdot \sin^2(\delta/2)} \quad (7)$$

For angle of incidence $\alpha = 0$ (or: infinitely expanded plates) the following results for the phase difference:

$$\delta = \frac{2 \cdot d \cdot k}{\cos \alpha} = 2 \cdot d \cdot k$$

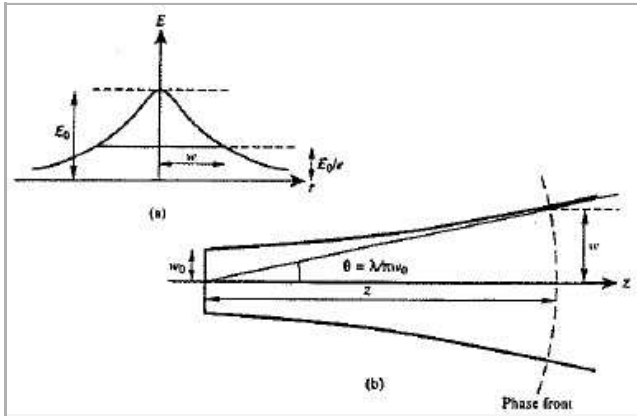


Fig. 6: Characteristics for a Gaussian beam. (a) Gaussian amplitude distribution for a constant phase front. (b) Beam contour with the hyperbolic beam envelopes of the expanding beam and the asymptotic angle θ .

Substituting in Equation (7), the following results for the intensity I (standardised for the initial input intensity I_0):

$$I = I_0 \cdot \frac{(1-R)^2}{(1-R)^2 + 4 \cdot R \cdot \sin^2\left(\frac{2\pi}{\lambda} \cdot d\right)} \quad (8)$$

where $k = 20\pi/\lambda$.

This function was named after G.B. Airy and is illustrated in Fig. 3 as a function of $k \cdot d$ and for different reflection factors R of the mirrors (with wave number $k = 2\pi/\lambda$). Using the so-called finesse coefficient K , Equation (8) can be somewhat more lucidly presented :

$$T_1 = \frac{I}{I_0} = \frac{1}{1 + K \sin^2(k \cdot d)} \quad (9)$$

with

$$K = \left(\frac{2 \cdot r}{1 - r^2}\right)^2$$

where $r = \sqrt{R}$ and $T_1 =$ transmission of intensity.

In this case, the separation of the maxima is of importance in a measuring technological context:

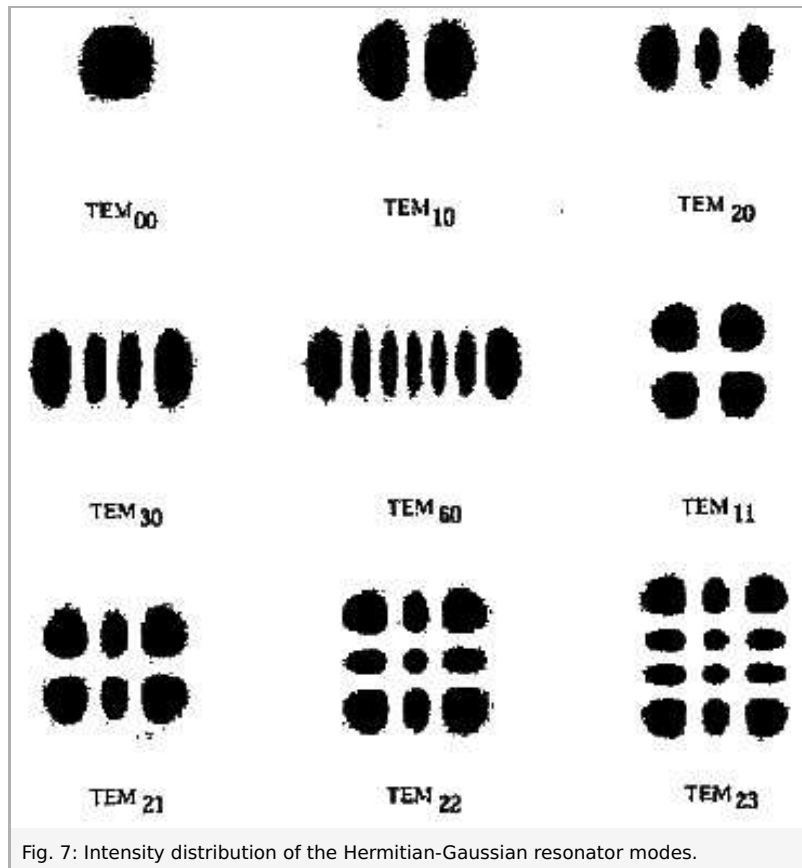


Fig. 7: Intensity distribution of the Hermitian-Gaussian resonator modes.

If there is a maximum (or complete) transparency, the wavelength cannot be definitively determined, since any wavelength having

$$n\pi = k_n d = \frac{2\pi}{\lambda_n} \cdot d \text{ or } n \cdot \frac{\lambda_n}{2} = d \quad (10)$$

can be valid when n is whole number.

According to Equation (10), the frequency difference $\delta\nu$, between two maxima of the transmission with λ_n and λ_{n+1} is then given by :

$$\delta\nu = \frac{c}{2d}; c = \text{speed of light} \quad (11)$$

This frequency difference is also termed the free spectral range (FSR).

Another important characteristic parameter of the FabryPerot interferometers is the finesse F , which specifies how many lines can be resolved in a free spectral range:

$$F = \frac{\delta\nu}{\Delta\nu} \quad (12)$$

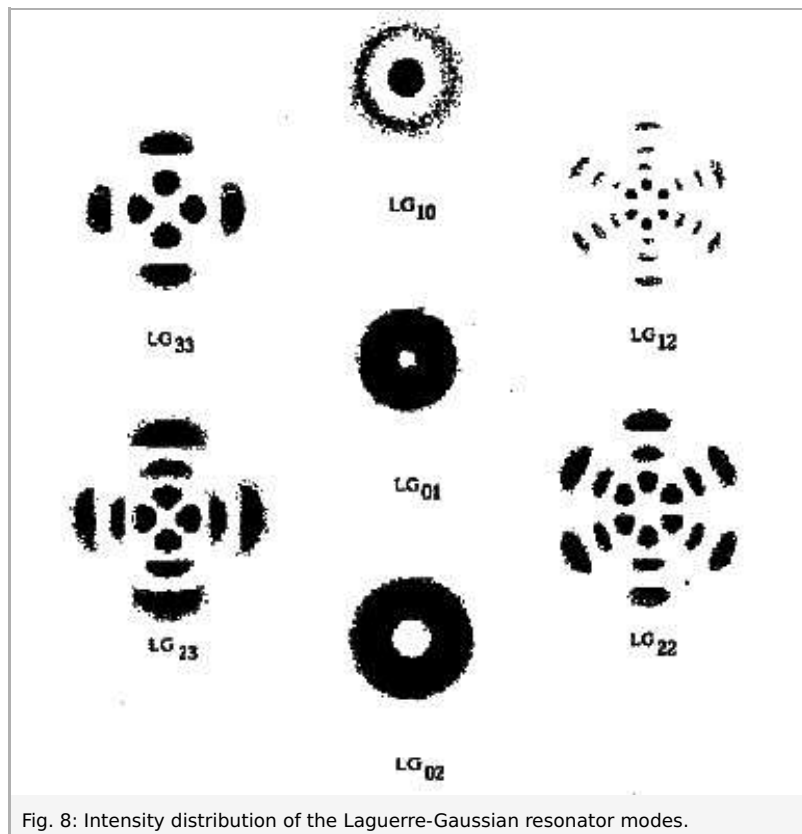


Fig. 8: Intensity distribution of the Laguerre-Gaussian resonator modes.

In this context, $\Delta\nu$ is the half-value width of a transmission range (thus the total frequency width in which the half-value width T_1 is greater than or equal to 1/2). With the aid of Equation (8) and Fig.3, it can be seen that this parameter is only applicable for larger reflection factors. The finesse F can be expressed by using parameters $r = \sqrt{R}$ and d of the interferometers. Combining

$$T_1^{(1/2)} = \frac{1}{2} = \frac{1}{1 + K \sin^2(k_h \cdot d)}$$

with

$$k_h = \frac{2\pi}{\lambda_h} = \frac{\pi \cdot \Delta\nu}{c}$$

the following is obtained for large values of r and consequently for narrow transmission regions (thus, the approximation: $\sin(k_h \cdot d) \propto k_h \cdot d$):

$$F = \frac{\delta\nu}{\Delta\nu} = \frac{\pi \cdot r}{1 - r^2} = \frac{2\pi \cdot \sqrt{K}}{4} \quad (13)$$

\,

On the mode spectrum:

The Fabry-Perot interferometer is generally an *optical resonator*.

To be able to form oscillation modes within this resonator, it must be stable with respect to its resonance capability.

To illustrate the stability properties of the resonator, the beam path of the light between the mirrors can be demonstrated by a row of lenses separated by the mirror distance d ; whereby the beam may not leave the regions of the lenses in the progressive course if a stable resonance is to be formed (Fig. 4). In our case, a plane mirror and a concave one with a radius of curvature of $p = 1.4 \text{ m}$ are used.

In this picture, the plane mirror is depicted as a plane that has no influence on the light beam and the concave mirror, by a lens with

$$f = \frac{p_2}{2}$$

In general, the following stability condition for the resonator results from this depiction:

$$0 \leq g_1 \cdot g_2 \leq 1$$

with

$$g_1 = \left(1 - \frac{d}{\rho_1}\right)$$

$$g_1 = \left(1 - \frac{d}{\rho_1}\right) \quad (14)$$

$$g_2 = \left(1 - \frac{d}{\rho_2}\right)$$

In our case $g_1 = 1$ (for a plane mirror with $\rho_1 = \infty$ and $g_2 \leq 1$ (for the concave mirror). Thus, this criterion is fulfilled. In Fig. 5 the stability diagram is shown.

To investigate the shape of the modes, we must consider the temporal development of an arbitrary initial amplitude distribution of the \vec{E} field vector (in any arbitrary initial plane with $z = z_0 = 0$) within the resonator:

$$u(x, y, z, t) = \text{Re}[u(x_0, y_0) e^{i(\omega t - kz)}]$$

To obtain the time-independent modes (static solution), the following Huygens' integral must be solved:

$$u(x, y, t) = \frac{i}{\lambda} \iint u_0(x_0, y_0, z_0) \frac{1 + \cos \alpha}{2} \cdot \frac{e^{-ik|\vec{r} - \vec{r}_0|}}{|\vec{r} - \vec{r}_0|} dx_0 dy_0 \quad (15)$$

where α represents the angle between \vec{r} and \vec{r}_0 with reference to the z axis. For incident radiation close to the axis, (15) simplifies with

$$\frac{1 + \cos \alpha}{2} \approx 1 \text{ and } |\vec{r} - \vec{r}_0| \approx d.$$

In addition, the Fresnel approximation can be substituted for

$$k \cdot |\vec{r} - \vec{r}_0| = k \left[(z - z_0)^2 + (x - x_0)^2 + (y - y_0)^2 \right]^{1/2} \approx k \cdot \left[d + \frac{(x - x_0)^2}{2d} + \frac{(y - y_0)^2}{2d} + \dots \right].$$

A Gaussian amplitude distribution in an arbitrary initial plane z_0 exhibits the property that it again becomes a Gaussian plane wave (Gaussian amplitude distribution and planar phase surfaces) in any arbitrary plane z (see Fig.6).

The radial amplitude distribution in the $x - y$ plane with $r^2 = x^2 + y^2$ is:

$$u(r) = \frac{\omega_0}{\omega} \cdot \exp \left[-i(kz - \phi) - r^2 \left(\frac{1}{\omega^2} + \frac{ik}{2R} \right) \right] \quad (16)$$

With the following quantities:

$$\omega^2 = \omega_0^2 \left[1 + \left(\frac{\lambda z}{u \omega_0^2} \right)^2 \right]$$

$$R = z \left[1 + \left(\frac{\pi \omega_0^2}{\lambda z} \right)^2 \right]$$

and the phase factor:

$$\phi = \tan^{-1} \left(\frac{\lambda z}{\pi \omega_0^2} \right)$$

In an arbitrary plane the radial intensity distribution can be described by a Gaussian slope function in the following manner:

$$I(r) = I_0 \cdot e^{-2r^2/\omega^2}$$

whereby the width ω of the Gaussian beam changes with progression in the z direction.

In addition to this fundamental solution of the integral equation (15), still other solutions exist which are also characterised by a Gaussian intensity distribution. They are modes of higher orders, whose appearance depends on the symmetry conditions:

1. If this is a system with Cartesian symmetry, the amplitude distribution results from the Hermitian-Gaussian modes to:

$$U_{mn}(r, z) = \frac{\omega_0}{\omega} H_m \left(\sqrt{2} \frac{x}{\omega} \right) H_n \left(\sqrt{2} \frac{y}{\omega} \right) \exp \left[-i(kz - \phi) - r^2 \left(\frac{1}{\omega^2} + \frac{ik}{2R} \right) \right] \quad (17)$$

with the phase factor:

$$\phi = (m + n + 1) \tan^{-1} \left(\frac{\lambda z}{\pi \omega_0^2} \right) \quad (18)$$

where H_m and H_n are the Hermitian polynomials.

The phase variation ϕ means that the phase velocity sinks with the mode's order and thus different resonance frequencies exist for the different modes. The intensity distribution $I(x, y)$ is shown in Fig.7.

2. In a cylindrical symmetry of the system, the following amplitude distributions result for the modes:

$$|E_{p,l}(r, \Theta, z)| = E_0 \left(\sqrt{2} \frac{r}{\omega} \right)^l \cdot L_p^l \left(2 \frac{r^2}{\omega^2} \right) \cdot \exp \left[-i(kz - \Phi) - r^2 \left(\frac{1}{\omega^2} + \frac{ik}{2R} \right) \right] \cdot \cos(l\Theta) \quad (19)$$

with the phase factor:

$$\Phi(p, l, z) = (2p + l + 1) \tan^{-1} \left(\frac{\lambda z}{\pi \omega_0^2} \right) \quad (20)$$

In this case, L_p^l represents the Laguerre polynomials.

The amplitude distributions of these modes are shown in Fig.8. The phase factor (20) causes the phase velocities, and thus the resonance frequencies of the different modes, to be different. Additional boundary conditions of the system result in the resonator's higher modes are of the Cartesian or cylindrically symmetrical type. However, for the present set-up these are not predetermined; therefore, both types are possible.

The resonance frequencies are thus given by the following:

$$\nu_{qmn} = \left[q + (m + n + 1) \frac{\cos^{-1}(\sqrt{g_1 g_2})}{\pi} \right] \frac{c}{2 \cdot d} \quad (21)$$

for Cartesian co-ordinates and

$$\nu_{qpl} = \left[q + (2p + l + 1) \frac{\cos^{-1}(\sqrt{g_1 g_2})}{\pi} \right] \frac{c}{2 \cdot d} \quad (22)$$

for cylindrical co-ordinates with the designations used above.